ACS OMEGA

http://pubs.acs.org/journal/acsodf

Article

New Alloy of an Al-Chalcogen System: AlSe Surface Alloys on Al(111)

Enze Shao,[#] Kai Liu,[#] Hao Xie, Kaiqi Geng, Keke Bai, Jinglan Qiu, Jing Wang, Wen-Xiao Wang,* and Juntao Song*

Cite This: *ACS Omega* 2022, 7, 45174−45180

Read Online

ACCESS | Metrics & More | Article Recommendations | Supporting Information

ABSTRACT: Metal chalcogenides are a promising material for novel physical research and nanoelectronic device applications. Here, we systematically investigate the crystal structure and electronic properties of AlSe alloys on Al(111) using scanning tunneling microscopy, angle-resolved photoelectron spectrometry, and first-principle calculations. We reveal that the AlSe surface alloy possesses a closed-packed atomic structure. The AlSe surface alloy comprises two atomic sublayers (Se sublayer and Al sublayer) with a height difference of 1.16 Å. Our results indicate that the AlSe alloy hosts two hole-like bands, which are mainly derived from the in-plane orbital of AlSe (p_x and p_y). These two bands located at about −2.22 ±0.01 eV around the Gamma point, far below the Fermi level, distinguished from other metal chalcogenides and binary alloys. AlSe alloys have the advantages of large-scale atomic flat terraces and a wide band gap, appropriate to serve as an interface layer for two-dimensional materials. Meanwhile, our results provide implications for related Al-chalcogen interfaces.

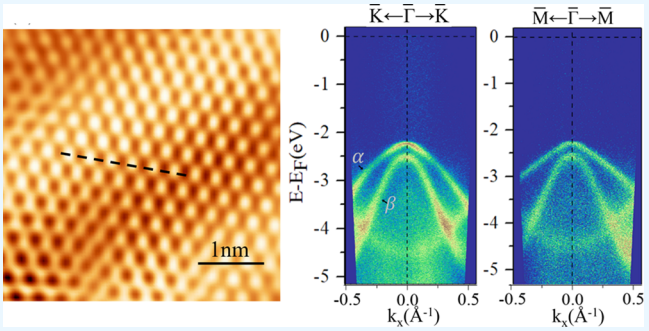

INTRODUCTION

Transition metal dichalcogenides (TMDCs) comprising transition metal atoms, like Mo or W, and chalcogen atoms, such as S, Se, or Te, have emerged as promising materials for diverse applications such as optics, nanoelectronics, and sensing. TMDCs are a diverse group whose properties vary from semiconducting to metallic. Semiconducting TMDCs like MoS_2 could serve as high quantum efficiency optoelectronic and valleytronic devices.[1−3] Metal TMDCs, like $NbSe_2$ and $TaSe_2$, have attracted immense attention because of their rich physical properties, especially superconductivity and charge density waves (CDW).[1,4−7]

Other than metal dichalcogenides, metal monochalcogenide alloys, synthesized by direct selenization or tellurization of metal substrates, are also emerging, such as CuSe, AgTe, and AgSe.[8−11] They exhibit abundant structural and physical properties. AgTe and AgSe display closed-packed atomic structures with a $(\sqrt{3} \times \sqrt{3})$ structure. In addition, several metal monochalcogenide alloys show structures of chains, for example, Te on the Cu(111) system with $(2\sqrt{3} \times \sqrt{3})$ Cu−Te chains.[12−15] Recent angle-resolved photoemission spectroscopy (ARPES) measurements have reported that CuSe and AgTe possess two-dimensional Dirac nodal line fermions (its Dirac point extends along the $M - \Gamma - K$ high symmetry line, forming the Dirac nodal line), protected by the mirror reflection symmetry.[8,9,11] Moreover, chalcogen-based surface alloys are also promising substrates for epitaxial growth. For example, the CDW properties of $TiSe_2$ could be tuned by CuSe substrates.[16] As a common metal substrate, aluminum is simple and cheap. In addition, Al-chalcogen compounds are also intermediate products in Al-ion batteries. So far, the chalcogen-Al system has not been sufficiently studied, and it is not clear for S/Al(111) and Se/Al(111) alloys whether the structure of AlS and AlSe is planar or buckling.[17−19] It is reported that the AlSe interface layer could be formed during Al_2Se_3 epitaxial on the Si substrate.[20,21] Identifying the electronic properties of AlSe is especially a challenge due to the complex energy bands of the Si substrate. Here, we take Se/Al(111) alloy as an example to clarify the formation process and the structure of the chalcogen element/Al(111) system.

In this study, we systematically investigate the crystal structure and electronic properties of AlSe alloys on the Al(111) surface, combining the experiment with the calculation method. The atomic arrangement of AlSe on Al(111) is directly revealed using high-resolution scanning tunneling microscopy (STM). AlSe is characterized by a buckled structure. Reflection high-energy electron diffraction

Received: August 30, 2022
Accepted: November 16, 2022
Published: November 29, 2022

(RHEED) and X-ray photoelectron spectroscopy (XPS) measurements are also carried out to monitor the formation process of AlSe alloys and change in their chemical bonding. The interaction between the substrate and AlSe alloys gives rise to a band gap. This interplay is analyzed by using ARPES and density functional theory (DFT) calculations.

RESULTS AND DISCUSSION

Figure 1 shows the typical XPS spectra of the core level of Se 3d for AlSe alloys. There are two distinct peaks of Se $3d_{3/2}$ and

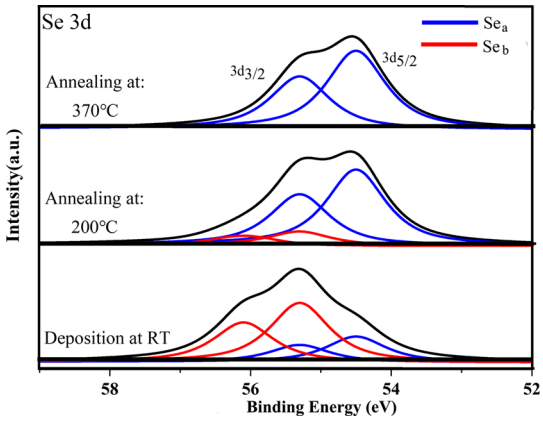

Figure 1. XPS spectra for Se 3d core levels at normal emission. Lower spectrum is obtained immediately after deposition. Upper two spectra are taken on the same sample after annealing at 200 and 370 °C, respectively. Red and blue solid peaks indicate the Voigt-type fitting results of the different chemical states of Se. Red peak represents Se bulk contribution (Se_b) and blue represents Se of AlSe alloy contribution (Se_a). Spectra were normalized to the same height.

Se $3d_{5/2}$ for Se 3d because of spin-orbit interactions. The lowest panel of Figure 1a shows the spectrum of Se 3d after deposition at room temperature. The characteristic peaks of Se can be fitted as four spectroscopic contributions. Two red peaks labeled as Se_{b1} and Se_{b2} at a binding energy of 56.10 and 55.31 eV correspond to the levels related to bulk Se atoms, in perfect accordance with previous studies.[10] This means that they come from chemical bonds characterized by Se−Se in Se bulk. The two blue peaks are labeled at binding energies of 55.30 and 54.60 eV. Compared with the binding energy of Se_{b1} and Se_{b2}, the binding energy of Se_{a1} and Se_{a2} is shifted by ΔE_{chem} = 0.8 eV. It indicates a charge transfer process between the substrate and Se atoms, after Se atoms deposition on Al(111). In other words, Se−Al bonds may be formed during Se adsorption on the Al(111) substrate. Therefore, the two chemical environments for Se deposition on Al(111) at room temperature include Se−Se and Se−Al bonds. The annealing process was taken out to get a single chemical environment. First, samples were annealed at 200 °C, which significantly changed the photoemission spectrum. The intensity of the Se_{a1} and Se_{a2} peaks increased. In contrast, Se_{b1} and Se_{b2} peaks (indicated Se−Se bond) were reduced, suggesting that the annealing process either evaporated the excess Se overlayer or promoted the Se interaction with Al. Then, the annealing temperature was elevated to 370 °C, and the peaks corresponding to the Se−Se bond (Se_{b1} and Se_{b2} peaks) entirely vanished. The only remaining peaks were related to the Se−Al bond (Se_{a1} and Se_{a2} peaks), signifying a single phase of the AlSe alloy layer formed on the surface. Moreover, the uniform XPS spectra taken at different areas of samples demonstrate the high quality of AlSe alloys.

On the other hand, the crystal symmetry of the AlSe alloy was detected by RHEED. Figure 2a,b shows typical RHEED

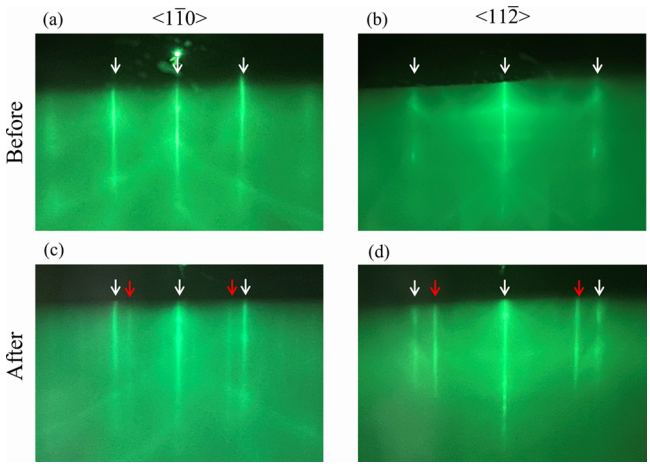

Figure 2. (a and b) RHEED images observed for the Al(111) substrate along $\langle 1\bar{1}0\rangle$ azimuth and $\langle 11\bar{2}\rangle$ azimuth. White arrows indicate the diffraction pattern from the Al(111) substrate. (c and d) RHEED images were observed after deposition and annealing at 370 °C in the same direction as (a and b). Red arrows indicate new patterns resulting from the AlSe alloy.

images of Al(111) before deposition. The stripes are bright and sharp, resulting from lattice diffraction along $\langle 1\bar{1}0\rangle$ and $\langle 11\bar{2}\rangle$ of the Al(111) surface. It means a clean and smooth surface. The deposition process was monitored by a film thickness monitor. When the thickness is about 0.75 monolayer (ML), additional streaks appear in the RHEED images and become sharper after annealing at 370 °C, indicated by red arrows shown in Figure 2c,d. These new stripes are ascribed to the AlSe alloy on the substrate. Only one set of patterns suggests the single direction of AlSe domains. During measurement, streaks induced by the AlSe alloy and the Al(111) substrate reappear when the sample is rotated by every 60°. Therefore, the AlSe alloy also has a threefold symmetry. The space between streaks of AlSe along the Al$\langle 11\bar{2}\rangle$ direction is $\sqrt{3}$ times larger than that along the Al$\langle 1\bar{1}0\rangle$ direction. Such a feature is the same as that of the Al(111) surface with a closed-packed atomic structure. These results imply the possibility of the closed-packed atomic structure for the AlSe surface alloy. In addition, the crystal orientation of the AlSe alloy aligns with the Al(111) surface in an epitaxial manner. The ratio of stripe spacing, for the Al(111) surface to AlSe alloy film along the Al $\langle 11\bar{2}\rangle$ direction, is estimated to be 1.337 ± 0.030. Accordingly, the lattice spacing of AlSe is preliminarily estimated to be about 0.383 ± 0.009 nm [0.286 nm × (1.337 ± 0.030) = 0.383 ± 0.009 nm]. Similarly, for the Al$\langle 1\bar{1}0\rangle$ direction, the lattice spacing of AlSe is deduced as 0.376 ±0.006 nm, which is comparable to that of the $\langle 11\bar{2}\rangle$ direction. The results of RHEED verify that the AlSe alloy is flat on a large scale. We will discuss the crystallographic structures in more detail by a combination of STM and DFT in the following.

STM measurements were taken to further confirm the symmetry and exact atomic structure of AlSe alloys. Figure 3a shows atoms of AlSe alloys arranged in a closed-packed atomic structure, which is similar to the structure of S atoms on the Al(111) substrate reported previously.[19] A profile line,

https://doi.org/10.1021/acsomega.2c05606
ACS Omega 2022, 7, 45174−45180

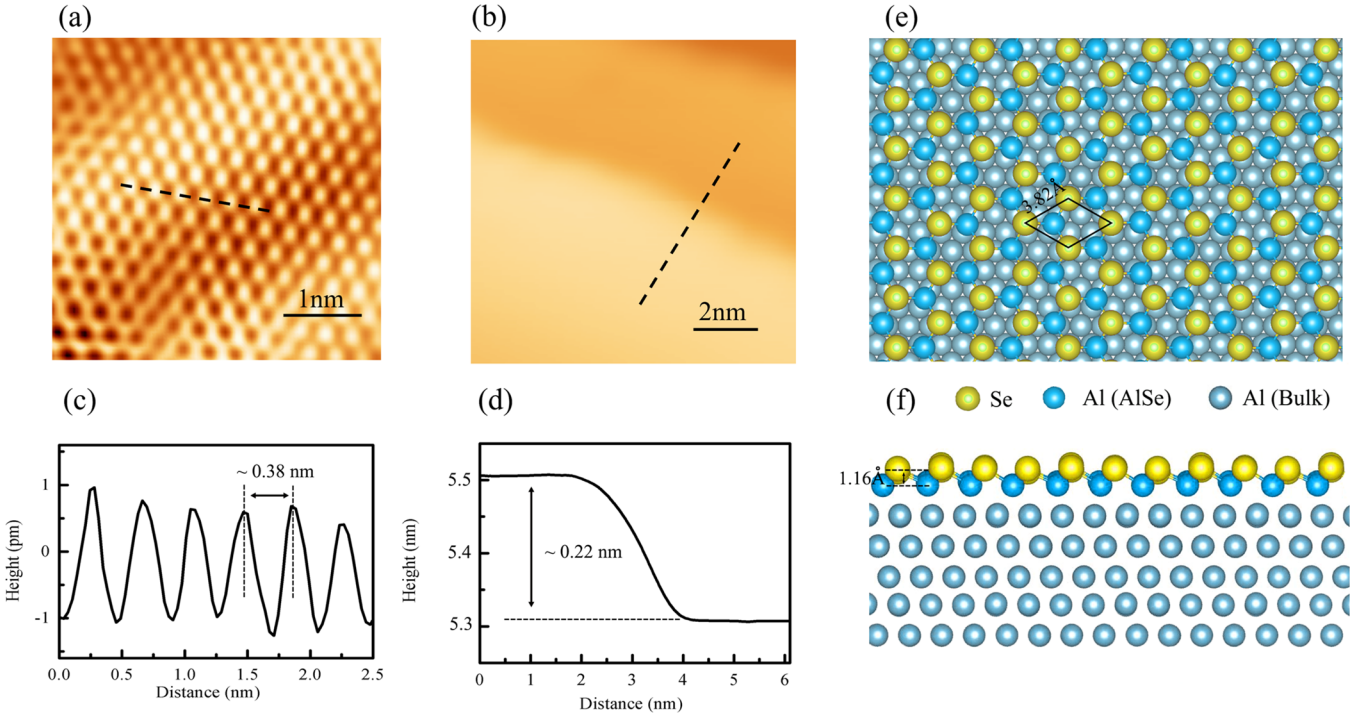

Figure 3. Atomic structure of the AlSe surface alloy on Al(111). (a) Typical atomic STM images of the AlSe alloy on Al(111) (V_s = 1.1 V, I = 130 pA). (b) STM topology of a terrace of the AlSe surface alloy on Al(111) (V_b = 1.1 V, I = 130 pA). (c and d) Height profiles from the black dashed lines in (a and b), respectively. Distance between the nearest atoms is 0.38 nm. (e and f) Top and side views of the buckled AlSe alloy model.

measured along the dotted line of the image in Figure 3a, shows a periodicity of 0.38 nm. This periodicity agrees quite well with RHEED results. The AlSe film continuously crosses the terraces of the substrate. The steps are estimated to be 0.22 nm high, attributed to the height of Al(111) steps, as illustrated in Figure 3b,d. However, we did not find isolated AlSe islands, suggesting that they prefer to distribute over a large surface scale. Such a feature has also been observed for Te deposited on Ag (111)[8,11] and many other alloys.[22−24] These results also provide the proof of the atomically flat AlSe alloy on Al(111) surfaces, which is one of the advantages for AlSe to be used as substrates.

First-principles calculations further confirm the closed-packed atomic structure of the AlSe alloy. A slab model, including the substrate, is shown in Figures 3 and S3 in the Supporting Information. The fully relaxed AlSe exhibits two stable phases: the planar phase with a lattice constant of 4.4 Å and the buckled phase with a lattice constant of 3.82 Å. We can ascertain the buckled phase of our AlSe sample from two aspects. One, from the calculation, the buckled phase of AlSe has lower formation energy than the planar phase (see Figure S2). Therefore, the buckled phase is preferential in terms of thermodynamics. Second, the calculated lattice constant of the buckled AlSe phase well agrees with STM and REED results. In detail, the 3 × 3 supercell for buckled AlSe (3.82 Å ×3 = 11.46 Å) nearly commensurates with the 4 × 4 Al(111) surface supercell (2.86 Å ×4 = 11.44 Å). There is only a 0.17% mismatch. This excellent agreement between experiments and calculations confirms the successful synthesis of the buckled AlSe alloy with high quality. Figure 3e,f shows the top and side views of the corresponding AlSe model, in good agreement with STM images. Different from planar AgTe and AgSe alloys with a $(\sqrt{3} \times \sqrt{3})R30^\circ$ structure, the AlSe alloy has a buckled structure including two atomic sublayers, the Al sublayer and the Se sublayer, with a height difference of 1.16 Å, as marked in Figure 3e,f. This buckled structure is surprisingly similar with the AlSe/GaSe on Si(111), in which the buckled height is 1.13 ± 0.02 Å and the lattice constant is 0.384 nm.[20,21,25] First, it may due to the lattice match of AlSe with substrates. The period of 0.38 nm match about $\sqrt{2}/2$ times the atom distance for the unreconstructed Si(111) surface, 4/3 times that of the Al(111) surface. Another contributing factor may be the strong interaction of the substrates with AlSe. Si atoms bonding with Al/Ga atoms, similar to Al(111) bulk, significantly affect the sites of Al atoms of the AlSe alloy.

Figure 4 shows the band structure of AlSe on Al(111), probed by ARPES with a photon energy of 21.2 eV. An electron-like band appears along high symmetry directions, with its bottom at about −4.65 ± 0.04 eV at the Γ point. This state is the surface state of Al(111), consistent with the previous results by ARPES [1]. After being covered by the AlSe alloy, the Al(111) substrate still shows a clear surface state band both along $\bar{K}\bar{\Gamma}\bar{K}$ and $\bar{M}\bar{\Gamma}\bar{M}$ directions, as shown in Figure 4a−c. Previous literature also found that the surface state of Al(111) still appeared after being covered by a few layers of films.[26−28] Other than the surface state of the Al(111) substrate, there are two hole-like parabolic-type bands labeled as α and β along $\bar{K}\bar{\Gamma}\bar{K}$ and $\bar{M}\bar{\Gamma}\bar{M}$ directions, which is attributed to the reconstruction of the Al(111) surface with Se. The slope of dispersion for both α and β bands along $\bar{K}\bar{\Gamma}\bar{K}$ is larger than that along $\bar{M}\bar{\Gamma}\bar{M}$ directions. The local maximum of the α band is about −2.22 ± 0.01 eV at the $\bar{\Gamma}$ point. The energy gap between the maximum of the α band and β band is 0.29 ±0.01 eV. The β band "crossing" the surface state at −4.00 ± 0.01 eV leads to its strong intensity, which may result from the resonance between the surface state of Al(111) and the β band. Furthermore, ARPES did not resolve Rashba-type spin splitting for AlSe due to the weak Rashba SOC of the small

https://doi.org/10.1021/acsomega.2c05606
ACS Omega 2022, 7, 45174−45180

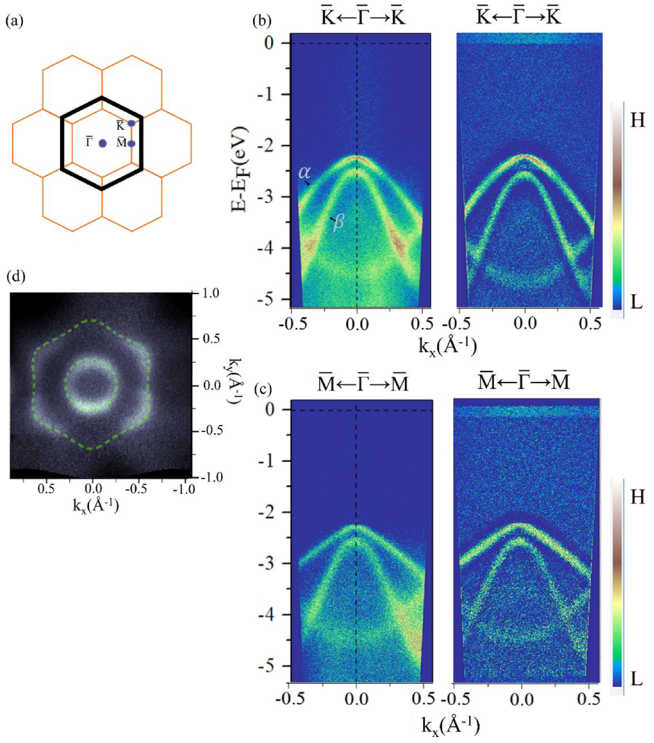

Figure 4. Electronic structure of the AlSe layer on Al(111), probed by ARPES with a photon energy of 21.2 eV. (a) Schematic surface Brillouin zone of the AlSe alloy and the Al(111) substrate. Black hexagon represents the SBZs of the Al(111). Yellow hexagons represent the SBZs of the AlSe alloy. (b and c) Left panel: Energy bands mapped along $\bar{K}-\bar{\Gamma}-\bar{K}$, $\bar{M}-\bar{\Gamma}-\bar{M}$ directions. Right panel: Corresponding maps of the second derivative of the ARPES intensity to the in-plane momentum. (d) Constant energy mapping of the AlSe alloy at −3 eV.

atomic number of both Al and Se. To better understand the structure of dispersive bands, we mapped the constant energy of bands shown in Figure 4c. The constant energy contour was taken at −3.00 ± 0.34 eV, centered at the $\bar{\Gamma}$ point of the first surface Brillouin zone. The constant energy contour also clearly shows α and β bands. The outer circle has a flower shape corresponding to the α band. The inner circle is attributed to the β band. These two parabolic-like band structures are also typical among other metal chalcogenide and binary alloys.[8,10,23] The difference of AlSe from others is that the top of its hole-like bands is very far away below the Fermi level. This feature means the semiconductor character of the AlSe alloy on Al(111). If the AlSe alloy serves as an interface between metal substrates and their overlayer materials, it may avoid strong interactions introduced by the metal substrates, such as avoiding the hybridization of electronic states near the Fermi level.

To investigate the origin of these energy bands, DFT calculations of dispersions for the monolayer buckled AlSe alloy on Al(111) are shown in Figure 5. The weights of different orbitals (p_x, p_y, p_z, s) for AlSe alloys are colored in red, blue, green, and purple, respectively. The calculated dispersions show that two hole-like bands are contributed from the AlSe alloy. Around −2.8 eV, the bands seem like crossing at the $\bar{\Gamma}$ point, which results from the back-folding of α and β bands due to reduced surface Brillouin zone in the calculation (for more discussion, see the Supporting Information). The projected band structures (Figure 5a) show that α/β bands are mainly contributed by the in-plane orbitals of AlSe (p_x, p_y). Furthermore, with SOC, the α and β bands split away 0.24 eV, also in accordance with the experimental separation of 0.29 ± 0.01 eV. The band structure mapping at −2.5 eV around the Γ point shown in Figure 5c quite well reproduces the experimental result indicated in Figure 4d, which is very similar to other binary alloys.[10,23,24] By carefully comparing the

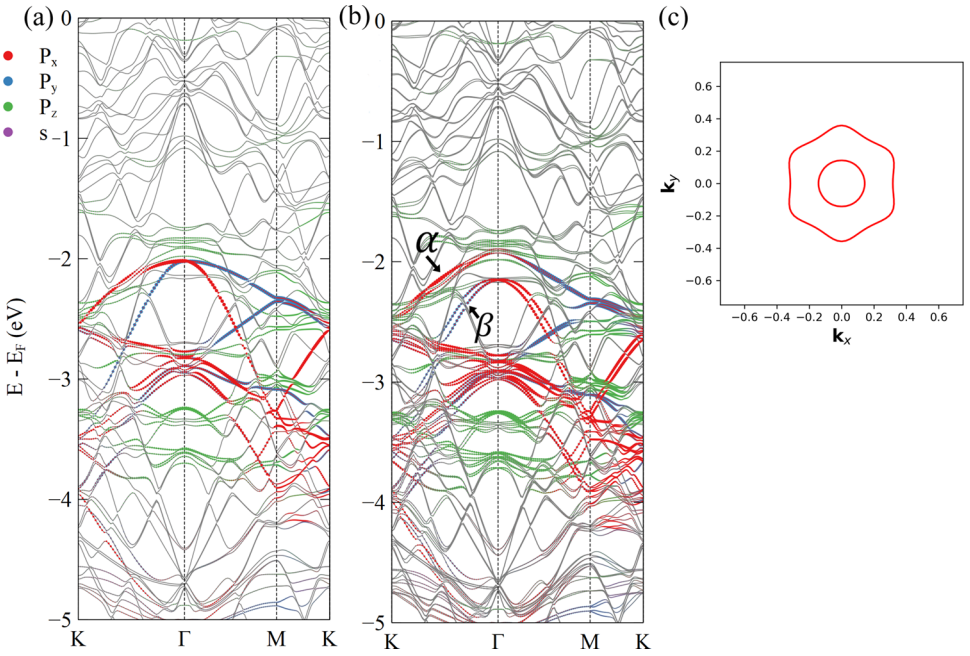

Figure 5. Calculated surface electronic structure of the relaxed AlSe alloy on Al(111) (a) without and (b) with SOC. Red, blue, green, and purple bands correspond to the projected band structures of AlSe, attributed to p_x, p_y, p_z, and s orbitals. Gray is contributed by the substrate. (c) Constant energy contours were calculated for the relaxed AlSe at −2.5 eV.

https://doi.org/10.1021/acsomega.2c05606
ACS Omega 2022, 7, 45174−45180

calculational and experimental bands, we find that the absolute energy location of α/β bands in the calculation is 0.3 eV, higher than the experimental data (2.22 ± 0.01 eV). This difference happened possibly because self-energy effects are not considered in the calculation.

For better understanding the band structure of AlSe, we also calculated the isolated AlSe layer, as shown in Figure S4. Besides α and β bands, there is one more narrow band across the Fermi level, labeled by black arrows in Figure S4a. This state is attributed to the out-of-plane orbitals of AlSe (p_z orbital), which is absent in the experiment. It is because the out-of-plane p_z orbital is sensitive to the coupling of the substrate and easily hybridized. Because of the strong coupling of the AlSe alloy and substrate, the p_z orbital is indistinguishable from substrate states and demonstrated by the DFT calculation with consideration of the substrate, as shown in Figures S4 and S5. According to the projected bands of the isolated AlSe layer, the upward dispersions in the range of the Fermi level to −6 eV are related to the p_z orbital. These bands are hybridized and become indistinguishable from substrate states, as demonstrated by our calculation and experiment shown in Figures 4 and 5. Previous literature reported that the isolated AlSe alloy has an electron-like band labeled as the γ band, crossing α and β bands.[17,18] We did not find the γ band of the AlSe alloy in the experiment and calculation. There are maybe two reasons. First, they did not consider the effect of the substrate that may tune the electronic properties of AlSe by strong coupling. Second, they use the planar model for calculation, which is different from our buckled structure.

The Si (111):AlSe and Si (111):GaSe also exhibit states resulting from the Al/Ga−Se bonds that occurred at about −2.7 eV and about −3 eV, respectively.[20,29] The deviation of the absolute energy location for these three systems may be due to the different elements and doping from the substrate atoms. Moreover, the bands related to p_z orbitals are also absent for the Si (111):GaSe system because of hybridization. There are also dissimilarities for AlSe on Al(111) and Si(111):AlSe/GaSe. For the latter two systems, the adlayers bonding with Si lead to a complex band structure that is difficult to distinguish the intrinsic band structure of AlSe and difficult to compare directly with calculation. Here, we provide a concise model of AlSe on the Al(111) system to investigate the electronic structure of the AlSe alloy.

Recently, it has been reported that the CDW properties of $TiSe_2$ could be tuned by the CuSe interface.[16] It shows that the metal chalcogenide is a good candidate as an interface to tune the properties of 2D materials. Substrates, especially metal substrates, may bring charge injection, strain, and charge carrier trapping to 2D materials. Atomic flat and dielectric substrates are beneficial for obtaining the intrinsic properties of 2D materials and transport measurements such as the hBN substrate. Different from its similar metal chalcogenide alloys such as CuSe, the AlSe alloy on Al(111) possesses a large band gap and a flat atomic surface on the substrate. Based on these characteristics, the AlSe alloy may be appropriate to be used as an intermediate transition layer. The AlSe alloy as a substrate could avoid the strong interaction between metal substrates and 2D materials. It is beneficial for achieving the intrinsic properties of 2D materials, which is a promising research direction.

CONCLUSIONS

In summary, we utilized high-resolution STM and ARPES to investigate the formation process of AlSe in detail and perform a comprehensive study to clarify the formation of Al−Se bonds. The Al atoms on the surface reconstruct and bond with Se to form a buckled AlSe alloy. According to STM and RHEED, AlSe has a closed-packed atomic arrangement aligning with the Al(111) surface. The main band of AlSe at $\bar{\Gamma}$ is two parabolic-like bands with negative dispersion. Based on the calculation, these two bands mainly derive from the in-plane orbital of AlSe (p_x and p_y). Furthermore, AlSe is atomically flat on a large scale. It has a wide energy band gap near the Fermi level, which make it potential as an interface to avoid the strong interaction introduced by the metal substrate for 2D materials and result in intrinsic 2D materials with excellent properties.

EXPERIMENTAL METHODS

Synthesis of AlSe. The Al(111) surface was prepared by repeated cycles of Ar^+ sputtering and annealing at 450 °C in UHV. The surface cleanliness was controlled by in situ high-resolution XPS on the impurity core levels and RHEED on the sharp and consecutive stripe. XPS was carried out using a DA30 electron energy analyzer (Scienta Omicron) and monochromatized Al Kα with 1486.7 eV photon energy and 100 eV pass energy. High-purity Se (99.99%, Sigma-Aldrich) was evaporated from a Knudsen cell with a temperature of 115 °C. The substrate was kept at room temperature during 10 min deposition, in an MBE chamber with a pressure lower than 4×10^{-10} torr. The process of deposition was monitored by RHEED and a thickness monitor.

Sample Characterization. ARPES experiments (Scienta Omicron DA30) were performed with He I $h\nu$ = 21.2 eV radiation from a high-brightness monochromatized commercial helium lamp. The base pressure was maintained below 5×10^{-11} torr during ARPES measurements, and the temperature was 10 K. On the other hand, samples were transferred by the UHV suitcase chamber for STM measurement at 77 K with an electrochemically etched W tip. The base pressure of the STM system (CreaTec) is better than 8×10^{-11} mbar.

First-Principles Calculations. First-principles calculations were performed using the Vienna *ab initio* simulation package,[30] with the Perdew−Burke−Ernzerhof (PBE) exchange and correlation function.[31] The electron wavefunctions were expanded on a plane wave basis with a kinetic energy cutoff of 400 eV, and the Brillouin zone was sampled by the Monkhorst−Pack *k*-mesh with a density of $2\pi \times 0.02$ Å^{-1}. The slab model of monolayer AlSe on the top of three layers of the Al(111) surface was used for simulating the interfacial interaction between them. A 20 Å vacuum layer was applied along the *z*-direction to avoid interactions between images.

ASSOCIATED CONTENT

Supporting Information

The Supporting Information is available free of charge at https://pubs.acs.org/doi/10.1021/acsomega.2c05606.

XPS spectra of core-level Al 2p; energy and buckling height versus lattice constant; simulated model of buckled AlSe on Al(111); calculated band structure of isolated AlSe without the Al(111) substrate; and discussion of back-folding bands (PDF)

https://doi.org/10.1021/acsomega.2c05606
ACS Omega 2022, 7, 45174−45180

AUTHOR INFORMATION

Corresponding Authors

Wen-Xiao Wang − *College of Physics and Hebei Advanced Thin Films Laboratory, Hebei Normal University, Shijiazhuang, Hebei 050024, China*; orcid.org/0000-0002-3728-5885; Email: wangwx@hebtu.edu.cn

Juntao Song − *College of Physics and Hebei Advanced Thin Films Laboratory, Hebei Normal University, Shijiazhuang, Hebei 050024, China*; Email: jtsong@hebtu.edu.cn

Authors

Enze Shao − *College of Physics, Hebei Normal University, Shijiazhuang, Hebei 050024, China*

Kai Liu − *College of Physics, Hebei Normal University, Shijiazhuang, Hebei 050024, China*

Hao Xie − *College of Physics, Hebei Normal University, Shijiazhuang, Hebei 050024, China*

Kaiqi Geng − *College of Physics, Hebei Normal University, Shijiazhuang, Hebei 050024, China*

Keke Bai − *College of Physics, Hebei Normal University, Shijiazhuang, Hebei 050024, China*

Jinglan Qiu − *College of Physics and Hebei Key Laboratory of Photophysics Research and Application, Hebei Normal University, Shijiazhuang, Hebei 050024, China*; orcid.org/0000-0001-6982-1120

Jing Wang − *College of Physics, Hebei Normal University, Shijiazhuang, Hebei 050024, China*

Complete contact information is available at: https://pubs.acs.org/10.1021/acsomega.2c05606

Author Contributions

#E.S. and K.L. contributed equally to this study.

Notes

The authors declare no competing financial interest.

ACKNOWLEDGMENTS

We thank Hongbo Wu and Xiaochuan Ma for useful discussions. This work was supported by the National Natural Science Foundation of China (Grant Nos. 11904076 and 11874139), the Natural Science Foundation of Hebei (Grant No. A2019205313), the Key Program of Natural Science Foundation of Hebei Province (Grant No. A2021205024), and the Science Foundation of Hebei Normal University (Grant No. L2019B10).

REFERENCES

(1) Yu, S.; Nakamura, Y.; Bahramy, M. S.; Kohama, Y.; Ye, J.; Kasahara, Y.; Nakagawa, Y.; Onga, M.; Tokunaga, M.; Nojima, T. Superconductivity protected by spin−valley locking in ion-gated MoS_2. *Nat. Phys.* **2015**, *12*, 144−149.

(2) Lopez-Sanchez, O.; Lembke, D.; Kayci, M.; Radenovic, A.; Kis, A. Ultrasensitive photodetectors based on monolayer MoS_2. *Nat. Nanotechnol.* **2013**, *8*, 497−501.

(3) Wang, Q. H.; Kalantar-Zadeh, K.; Kis, A.; Coleman, J. N.; Strano, M. S. Electronics and optoelectronics of two-dimensional transition metal dichalcogenides. *Nat. Nanotechnol.* **2012**, *7*, 699−712.

(4) Xi, X.; Zhao, L.; Wang, Z.; Berger, H.; Forrã, L.; Shan, J.; Mak, K. F. Strongly enhanced charge-density-wave order in monolayer $NbSe_2$. *Nat. Nanotechnol.* **2015**, *10*, 765−769.

(5) Schaibley, J. R.; Yu, H.; Clark, G.; Rivera, P.; Ross, J. S.; Seyler, K. L.; Yao, W.; Xu, X. Valleytronics in 2D materials. *Nat. Rev. Mater.* **2016**, *1*, 16055.

(6) Manzeli, S.; Ovchinnikov, D.; Pasquier, D.; Yazyev, O. V.; Kis, A. 2D transition metal dichalcogenides. *Nat. Rev. Mater.* **2017**, *2*, 17033.

(7) Xu, X.; Yao, W.; Xiao, D.; Heinz, T. F. Spin and Pseudospins in Transition Metal Dichalcogenides. *Nat. Phys.* **2014**, *10*, 343.

(8) Liu, B.; Liu, J.; Miao, G.; Xue, S.; Zhang, S.; Liu, L.; Huang, X.; Zhu, X.; Meng, S.; Guo, J.; Liu, M.; Wang, W. Flat AgTe Honeycomb Monolayer on Ag(111). *J. Phys. Chem. Lett.* **2019**, *10*, 1866−1871.

(9) Gao, L.; Sun, J. T.; Lu, J. C.; Li, H.; Qian, K.; Zhang, S.; Zhang, Y. Y.; Qian, T.; Ding, H.; Lin, X.; Du, S.; Gao, H. J. Epitaxial growth of honeycomb monolayer CuSe with Dirac nodal line Fermions. *Adv. Mater.* **2018**, *30*, No. e1707055.

(10) Lu, J.; Gao, L.; Song, S.; Li, H.; Niu, G.; Chen, H.; Qian, T.; Ding, H.; Lin, X.; Du, S.; Gao, H.-J. Honeycomb AgSe Monolayer Nanosheets for Studying Two-dimensional Dirac Nodal Line Fermions. *ACS Appl. Nano Mater.* **2021**, *4*, 8845−8850.

(11) Shah, J.; Sohail, H. M.; Uhrberg, R. I. G.; Wang, W. Two-Dimensional Binary Honeycomb Layer Formed by Ag and Te on Ag(111). *J. Phys. Chem. Lett.* **2020**, *11*, 1609−1613.

(12) Kißlinger, T.; Schneider, M. A.; Hammer, L. Submonolayer copper telluride phase on Cu(111): Ad-chain and trough formation. *Phys. Rev. B* **2021**, *104*, No. 155426.

(13) Bouaziz, M.; Zhang, W.; Tong, Y.; Oughaddou, H.; Enriquez, H.; Mlika, R.; Korri-Youssoufi, H.; Chen, Z.; Xiong, H.; Cheng, Y.; Bendounan, A. Phase transition from Au−Te surface alloy towards tellurene-like monolayer. *2D Mater.* **2021**, *8*, No. 015029.

(14) Kißlinger, T.; Raabgrund, A.; Geldiyev, B.; Ammon, M.; Rieger, J.; Hauner, J.; Hammer, L.; Fauster, T.; Schneider, M. A. CuTe chains on Cu(111) by deposition of one-third of a monolayer of Te: Atomic and electronic structure. *Phys. Rev. B* **2020**, *102*, No. 155422.

(15) King, M. O.; McLeod, I. M.; Hesp, D.; Dhanak, V. R.; Kadodwala, M.; MacLaren, D. A. Growth and alloying of thin film Te on Cu(111). *Surf. Sci.* **2012**, *606*, 1353−1359.

(16) Song, Z.; Huang, J.; Zhang, S.; Cao, Y.; Liu, C.; Zhang, R.; Zheng, Q.; Cao, L.; Huang, L.; Wang, J.; Qian, T.; Ding, H.; Zhou, W.; Zhang, Y.-Y.; Lu, H.; Shen, C.; Lin, X.; Du, S.; Gao, H.-J. Observation of an Incommensurate Charge Density Wave in Monolayer $TiSe_2$/CuSe/Cu(111) Heterostructure. *Phys. Rev. Lett.* **2022**, *128*, No. 026401.

(17) Jacobi, K.; Auschwitz, C. V.; Kambe, K. Angle-Resolved UV photoemission studies of the two dimensional band structures of sulfur, selenium, and tellurium monolayers adsorbed on Aluminium(111). *Surf. Sci.* **1980**, *93*, 310−326.

(18) Bullett, D. W. Anomalous band broadening of adsorbed chalcogen monolayers on Al(111). *Surf. Sci.* **1981**, *102*, L1−L6.

(19) Wiederholt, T.; Brune, H.; Wintterlin, J.; Behm, R. J.; Ertl, G. Formation of two dimensional sulfide phases on Al(111). *Surf. Sci.* **1995**, *324*, 91−105.

(20) Adams, J. A.; Bostwick, A.; Ohta, T.; Ohuchi, F. S.; Olmstead, M. A. Heterointerface formation of aluminum selenide with silicon: Electronic and atomic structure of Si(111):AlSe. *Phys. Rev. B* **2005**, *71*, No. 195308.

(21) Lu, C.-Y.; Adams, J. A.; Yu, Q.; Ohta, T.; Olmstead, M. A.; Ohuchi, F. S. Heteroepitaxial growth of the intrinsic vacancy semiconductor Al_2Se_3 on Si(111): Initial structure and morphology. *Phys. Rev. B* **2008**, *78*, No. 075321.

(22) Tong, Y.; Bouaziz, M.; Zhang, W.; Obeid, B.; Loncle, A.; Oughaddou, H.; Enriquez, H.; Chaouchi, K.; Esaulov, V.; Chen, Z.; Xiong, H.; Cheng, Y.; Bendounan, A. Evidence of new 2D material: Cu_2Te. *2D Mater.* **2020**, *7*, No. 035010.

(23) Osiecki, J. R.; Uhrberg, R. I. G. Alloying of Sn in the surface layer of Ag(111). *Phys. Rev. B* **2013**, *87*, No. 075441.

(24) Wang, W.; Sohail, H. M.; Osiecki, J. R.; Uhrberg, R. I. G. Broken symmetry induced band splitting in the Ag_2Ge surface alloy on Ag(111). *Phys. Rev. B* **2014**, *89*, No. 125410.

(25) Rudolph, R.; Pettenkofer, C.; Bostwick, A. A.; Adams, J. A.; Ohuchi, F.; Olmstead, M. A.; Jaeckel, B.; Klein, A.; Jaegermann, W. Electronic structure of the Si(1 1 1):GaSe van der Waals-like surface termination. *New J. Phys.* **2005**, *7*, 108.

(26) Sato, Y.; Fukaya, Y.; Cameau, M.; Kundu, A. K.; Shiga, D.; Yukawa, R.; Horiba, K.; Chen, C.-H.; Huang, A.; Jeng, H.-T.; Ozaki, T.; Kumigashira, H.; Niibe, M.; Matsuda, I. Electronic structure of a

(3×3)-ordered silicon layer on Al(111). *Phys. Rev. Mater.* **2020**, *4*, No. 064005.
(27) Kubo, O.; Kinoshita, S.; Sato, H.; Miyamoto, K.; Sugahara, R.; Endo, S.; Tabata, H.; Okuda, T.; Katayama, M. Kagome-like structure of germanene on Al(111). *Phys. Rev. B* **2021**, *104*, No. 085404.
(28) Geng, D.; Yu, K.; Yue, S.; Cao, J.; Li, W.; Ma, D.; Cui, C.; Arita, M.; Kumar, S.; Schwier, E. F.; Shimada, K.; Cheng, P.; Chen, L.; Wu, K.; Yao, Y.; Feng, B. Experimental evidence of monolayer AlB_2 with symmetry-protected Dirac cones. *Phys. Rev. B* **2020**, *101*, No. 161407(R).
(29) Ohta, T.; Klust, A.; Adams, J. A.; Yu, Q.; Olmstead, M. A.; Ohuchi, F. S. Atomic structures of defects at GaSe/Si(111) heterointerfaces studied by scanning tunneling microscopy. *Phys. Rev. B* **2004**, *69*, No. 125322.
(30) Kresse, G.; Furthmuller, J. Efficient iterative schemes for ab initio total-energy calculations using a plane-wave basis set. *Phys. Rev. B* **1996**, *54*, 11169.
(31) Perdew, J. P.; Burke, K.; Ernzerhof, M. Generalized Gradient Approximation Made Simple. *Phys. Rev. Lett.* **1996**, *77*, 3865−3868.

https://doi.org/10.1021/acsomega.2c05606
ACS Omega 2022, 7, 45174−45180